Lithuanian Journal of Physics, Vol. 55, No. 4, pp. 305–314 (2015)
© Lietuvos mokslų akademija, 2015

REVIEW OF ELECTRON TRANSPORT PROPERTIES IN BULK InGaAs AND InAs AT ROOM TEMPERATURE

S. Karishy [a], P. Ziadé [a], G. Sabatini [b], H. Marinchio [b], C. Palermo [b], L. Varani [b], J. Mateos [c], and T. Gonzalez [c]

[a] *Ecole Doctorale de Sciences et Technologies, Université Libanaise, Fanar, Liban*
[b] *Institut d'Electronique et des Systèmes, CNRS UMR 5214, University of Montpellier, France*
[c] *Department of Applied Physics, University of Salamanca, Spain*
E-mail: luca.varani@umontpellier.fr

Received 29 September 2015; accepted 29 September 2015

A Monte Carlo simulation of electron transport in $In_{0.53}Ga_{0.47}As$ and InAs is performed in order to extract the main kinetic parameters: mean valley population, effective mass, drift velocity, mean energy, ohmic and differential mobility. Most of these quantities are crucial for the development of macroscopic numerical models. Moreover, for some calculated quantities, analytical interpolation equations are given in order to achieve easy implementation in numerical codes. A comparison between our Monte Carlo calculation and several experimental and theoretical calculations is also carried out in order to validate the results.

Keywords: Monte Carlo, transport, InGaAs, InAs

PACS: 72.20.Fr, 72.20.Ht, 72.80.Ey

1. Introduction

Nowadays nanoelectronics devices operating at ultrahigh frequencies have a huge number of applications in various domains: high-speed telecommunications, spectroscopy, imaging, security, THz-wave generation/detection systems [1].

Traditionally, the frequency response of the devices and their capacity of integration have improved by means of a progressive diminution of their size. Today the progress of technology has allowed one to reach characteristic dimensions in the nanometre range [2–6]. The fact that the technology allows the shrinking of the device dimensions towards the nanometric scale is useful in reducing the carrier transit time, thus generally improving the speed performances of traditional devices.

In parallel, the achievement of high-speed electronic devices requires semiconductor materials with excellent electron mobility and transport properties. Two examples of these materials are $In_{0.53}Ga_{0.47}As$ and InAs. The $In_{0.53}Ga_{0.47}As$ has been suggested to have a great potential for high-speed room-temperature devices due to high electron threshold velocities [7–9]. Moreover, recent studies showed that InGaAs transistors such as high electron mobility transistors (HEMTs) and metal–oxide–semiconductor field-effect transistors (MOSFETs) can be used as emitters or detectors in the THz domain [10, 11]. In the same context, the InAs, due to its low effective mass and a narrow gap, is a good prototype of material for future electronic devices. It is often used in combination with AlGaSb or AlSb in a wide range of electronic and optoelectronic applications. For example, an intrinsic cutoff frequency as high as 250 GHz at a drain voltage of 0.6 V has been achieved with a 0.1 μm gate length HEMT. Different attempts have also been made to design heterojunction bipolar transistors (HBTs) with InAs. Simple bipolar junction transistors (BJTs) and HBTs with an InAlAs or InAsP emitter have been studied, as well as more sophisticated HBTs made with InAs/AlSb superlattices. An InAs/AlSb quantum hot electron transistor (QHET) is another example of an innovative high-speed transistor [2] having the potential to efficiently exploit the unrivaled transport properties of InAs in THz applications. Despite the fact that InGaAs and InAs are very widely used in many different high frequency applications, a detailed study of their electronic transport is still limited [12–16].

In particular, the input parameters of the widely used hydrodynamic (HD) and drift–diffusion (DD) approaches are difficult to find, which leads to the difficulty of studying the behaviour of $In_{0.53}Ga_{0.47}As$ and InAs based devices using commercial or academic microscopic simulators. As a consequence, the first step to describe correctly both the stationary and transient regimes in $In_{0.53}Ga_{0.47}As$ and InAs is to extract the unavailable parameters using a microscopic simulation of the electronic transport. For this purpose, we perform a comprehensive investigation of transport parameters in $In_{0.53}Ga_{0.47}As$ and InAs at 300 K based on a Monte Carlo (MC) simulation.

The paper is organized as follows. In Section 2, the theoretical model is described. Then the following kinetic parameters are described: valley population in Section 3, effective mass in Section 4, average energy in Section 5, drift velocity in Section 6 and mobility in Section 7. The main conclusions are drawn in Section 8.

2. Theoretical model

In the framework of our MC simulation of charge transport in InGaAs and InAs, only the dynamic of electrons is taken into account. To investigate the transport properties of InGaAs and InAs at room temperature, we use a standard MC simulation [17, 18] where the electronic properties of the bulk material are directly related to the scattering mechanisms and the band structure. The input has been obtained interpolating the values of the corresponding binary materials [12, 19–22]. For the conduction band, we have used a model with three non-parabolic spherical valleys (one Γ, four equivalent L and three equivalent X). The scattering mechanisms which are included in the physical model are the following: collisions with ionized impurities (Brooks–Herring model), transitions due to absorption and emission of polar and non-polar optical phonons, collisions with acoustic elastic phonons, intervalley and alloy scatterings [23]. In particular, the impact ionization has been treated in the framework of the Keldysh approach [12, 24–27] where the probability per unit of time is given by

$$A(\epsilon) = \begin{cases} P\left(\dfrac{\epsilon - \epsilon_{\mathrm{th}}}{\epsilon_{\mathrm{th}}}\right)^2 & \text{if } \epsilon > \epsilon_{\mathrm{th}}, \\ 0 & \text{if } \epsilon < \epsilon_{\mathrm{th}}, \end{cases} \tag{1}$$

where A is a coeficient which indicates the strength of the scattering process and ϵ_{th} is a threshold energy. The parameter ϵ_{th} can be calculated using the Anderson and Crowell criteria [28] or following the procedure outlined by Quade et al. [29]. A is an adjustable parameter the value of which is chosen in order to reproduce the average ionization coefficient measured experimentally [30, 31].

Figure 1 shows the simulated impact ionization coefficient as a function of the inverse electric field, compared with several experimental and theoretical results available in the literature [30–36]. In the case of InGaAs, it can be clearly seen that the existing results differ by more than one order of magnitude for the same electric field. In our MC simulations, the input parameters have been adapted with

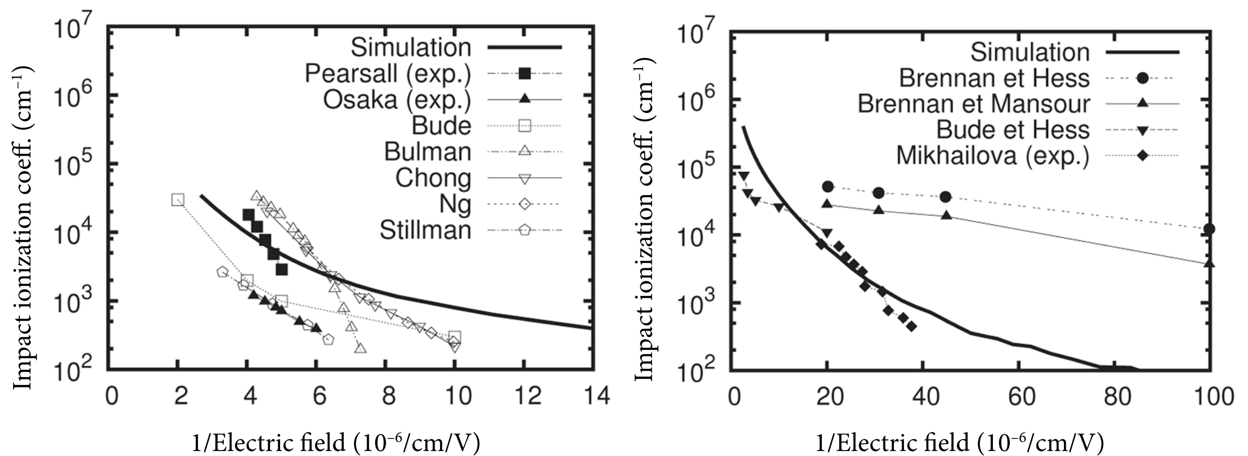

Fig. 1. Impact ionization coefficient as a function of inverse electric field in InGaAs (left) and InAs (right) with $N_D = 10^{16}$ cm^{-3}. The continuous lines represent MC simulation, the full symbols show the experimental results, and the empty symbols show other simulations present in the literature [30–39].

the experimental data of Pearsall [30]. In the case of InAs, because of the lack of experimental data, we have adapted our MC simulation to the experiments of Mikhailova [37]. Our MC results are also in good agreement with the simulations of Bude and Hess [32].

3. Valley population

We start the investigation of the bulk properties by calculating the fractional valley population in Γ, *L* and *X* valleys in steady-state conditions. The results are reported in Fig. 2 as functions of the electric field, for an electron density N_D equal to 10^{16} cm^{-3}. In the same figure, we have reported the theoretical results of Choo [34] for InGaAs and we observe a good agreement for all considered values of the electric field. For both materials, the electron transfer into the *L* valley starts at 1 kV/cm. Then, a greater quantity of electrons is found in the *L* valley compared to the Γ valley, starting at 11 kV/cm for InGaAs and 7 kV/cm for InAs. The transfers into the *X* valley begin around 6 kV/cm and 4 kV/cm, respectively. The electron population in the *X* valley becomes not negligible in both materials for electric fields greater than 30 kV/cm. In Fig. 2 we observe that, for InAs, the settlement of higher valleys takes place for weaker electric fields than for InGaAs because of the difference in the effective mass and the non parabolicity of the bands. The fractional valley population has been found to be practically independent of N_D in the range 10^{15}–10^{18} cm^{-3}, which is the domain studied in this article.

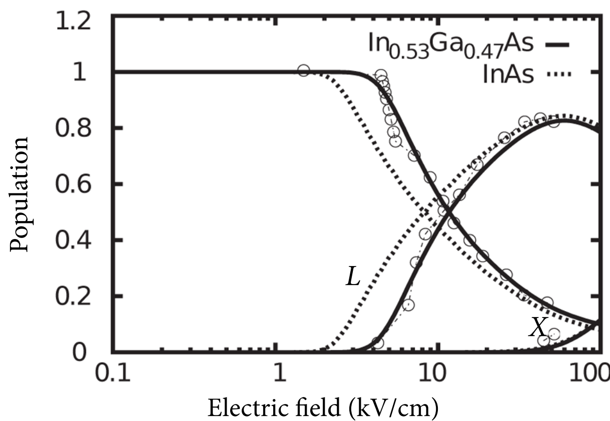

Fig. 2. Average fractional valley population of electrons in Γ, *L* and *X* valleys of InGaAs and InAs as a function of the electric field with $N_D = 10^{16}$ cm^{-3}. The lines represent MC simulation. The symbols represent the theoretical results of Choo [34]. The lines between symbols simply connect the reported points.

4. Effective mass

Figure 3 reports the results obtained for the mean longitudinal electron effective mass versus the electric field. This quantity is obtained by averaging the inverse electron longitudinal effective mass $1/m_x^*$ which, taking into account the non parabolicity of the bands, is deffined by

$$\frac{1}{m_x^*} = \frac{\partial^2 \epsilon}{\partial p_x^2} = \frac{1}{m^*(1+2\alpha\epsilon)}\left[1 - 2\alpha \frac{p_x^2}{m^*(1+2\alpha\epsilon)^2}\right], \qquad (2)$$

where p_x is the component of the moment in the direction of the electric field, α is the coeficient of non parabolicity, ϵ is the energy, and m^* is the electron effective mass at the bottom of the conduction band, that is, for an energy equal to zero. The longitudinal effective mass depends on the valley in which the electron is present.

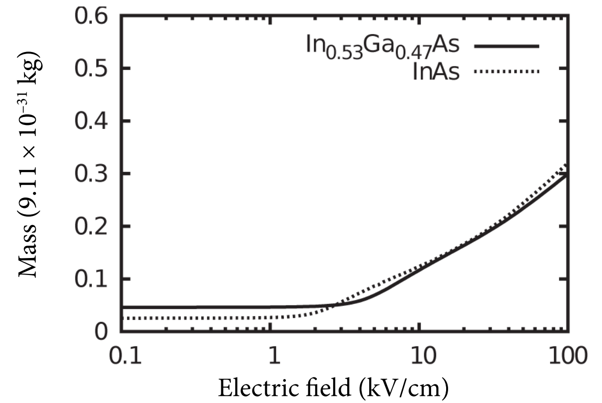

Fig. 3. Average electron effective mass of InGaAs and InAs as a function of the electric field for $N_D = 10^{16}$ cm^{-3}.

We observe three main zones depending on the electric field. The first zone is for values lower than the threshold field, where the majority of electrons are still in the Γ valley with a low average effective mass. The second area corresponds to the field values for which a significant number of electrons is transferred from the first to the second valley. The average effective mass increases towards the value of the effective mass in the *L* valley. Lastly, the third zone corresponds to the higher electric fields ($E \geq 30$ kV/cm) for which a significant number of electrons is progressively transferred into the *X* valley. The electron transfer between Γ and *L* valleys

is characterized by a larger electron mass difference than that between L and X valleys. This is the reason why the variation of the effective mass is higher for low electric fields.

Regarding the effective mass, in Fig. 4 we report our MC results compared with the experiments of Kesamanly [40] for InAs. A good agreement is found for the values of the electron density lower than 10^{17} cm^{-3} and a difference of about 20% is noted for higher electron densities around 10^{18} cm^{-3}.

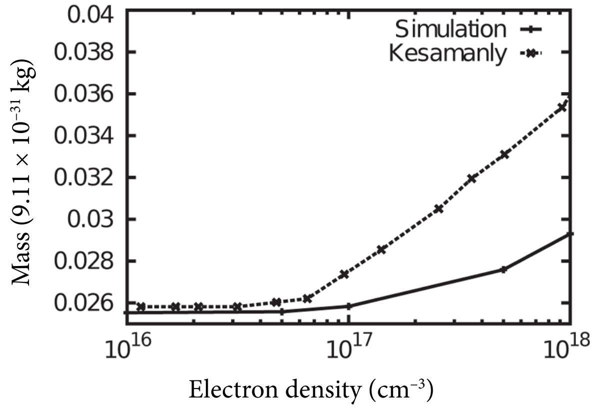

Fig. 4. Average electron effective mass of InGaAs as a function of electron density. The lines represent our MC simulation. The symbols represent the experimental results of Kesamanly [40]. The lines between the symbols simply connect the reported points.

5. Average energy

Figure 5 shows the average electronic energy as a function of the electric field, for $N_D = 10^{16}$ cm^{-3}. The behaviour of the average electronic density is dissimilar for lower and higher values of the electric field, for both InGaAs and InAs: the corresponding curves can be divided into two parts. The former one corresponds to low values of the electric field (<2 kV/cm), for which the electron mean energy remains nearly constant and equal to the value at thermodynamic equilibrium. In the latter one, corresponding to higher electric fields, the average energy increases with the electric field. As a matter of fact, as the field increases, the collisions become less effective in dissipating the energy brought to the electrons. Therefore, both the energy and the number of inelastic collisions increase until a new equilibrium is obtained in the hot carrier regime [41]. In the same figure, we have reported the theoretical results of Fischetti obtained for InGaAs and we observe a good agreement for electric fields lower than 20 kV/cm. The difference for higher fields results from the fact that Fischetti has used a full band model. Finally, for InAs we observe a good agreement with the theoretical results of Hori [42].

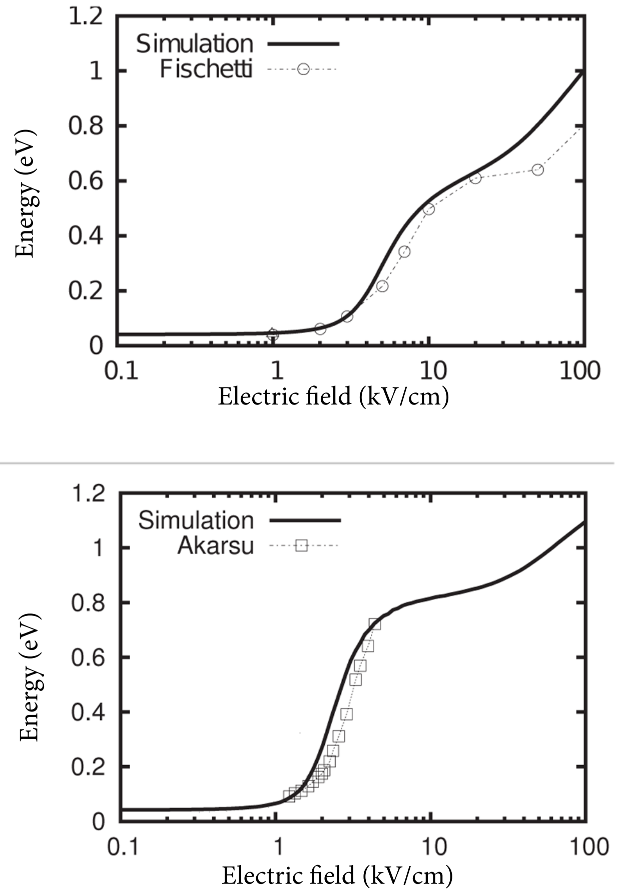

Fig. 5. Average energy as a function of the electric field in InGaAs (above) and InAs (below) with $N_D = 10^{16}$ cm^{-3}. The continuous lines represent MC simulation and the symbols show other simulations presented in the literature.

6. Drift velocity

The results obtained for the average electron velocity are reported in Figs. 6 and 7 as a function of electric field. The MC results are compared with different experimental and theoretical data present in the literature [13, 14, 42–51]. For an electric field lower than about 0.15 kV/cm, the velocity increases linearly and the carriers remain in the same valley (Fig. 2). As the electric field increases, carriers are transferred into higher valleys and the velocity becomes non-linear. In the hot carrier regime phonons are not able to thermalize electrons to the lattice

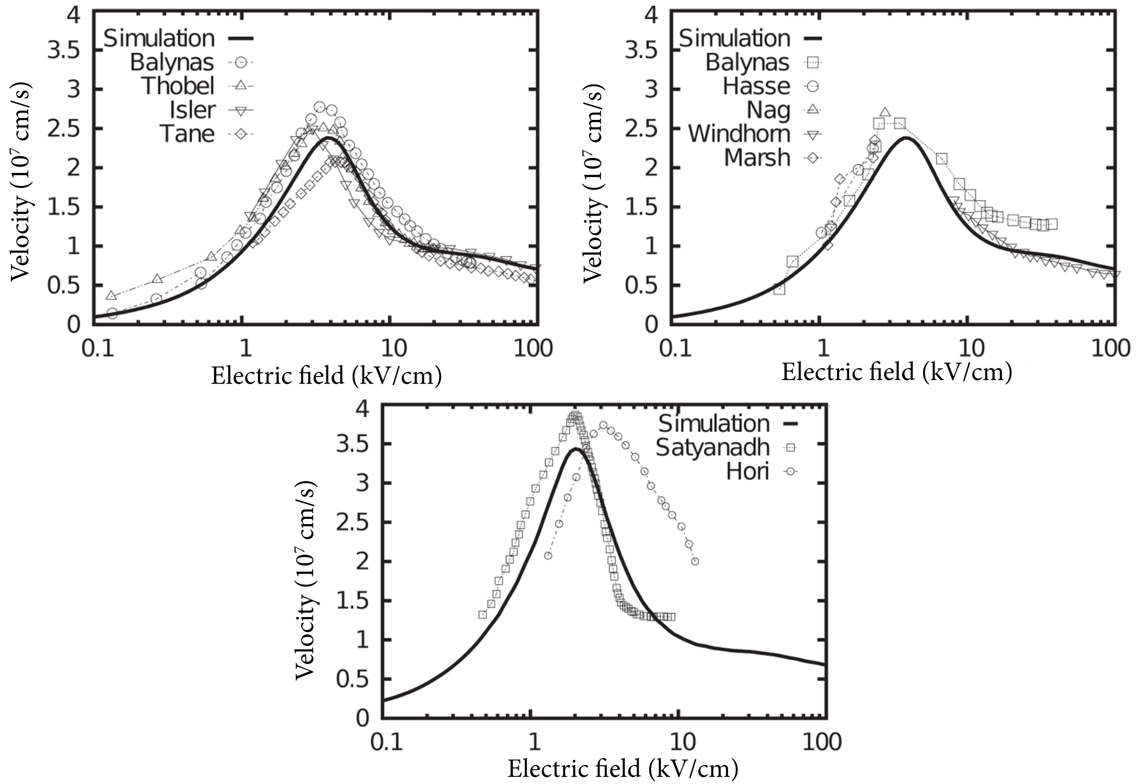

Fig. 6. Average electron velocity as a function of the electric field for InGaAs (top) and InAs (bottom) compared to several experimental (top left) [13, 43–47] and theoretical (top right, bottom) results [14, 46–49] present in the literature, with $N_D = 10^{16}$ cm^{-3}. The continuous lines represent MC simulations. The symbols show the experimental and theoretical results. The dotted lines simply connect the reported points.

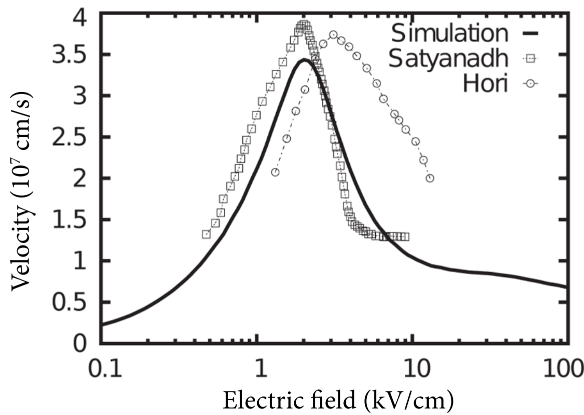

Fig. 7. Average electron velocity as a function of the electric field for InAs compared to theoretical results [42, 50] present in the literature, with $N_D = 10^{16}$cm^{-3}. The continuous line represents MC simulation. The dotted lines simply connect the reported points.

temperature; however, they limit the electron velocity. When the electrons are transferred from lower to higher valleys, their average effective mass increases (Fig. 3) and thus velocity starts to decrease. We notice that the velocity peak in InAs is about 3.5×10^7 cm/s for a threshold field of 2 kV/cm while it reaches a lower value of about 2.4×10^7 cm/s for a threshold field of 3.7 kV/cm in InGaAs. A decrease of the mean velocity can be noted for electric fields greater than 30 kV/cm due to the transfer of the electrons into the X valley.

It is useful to ot the velocity using analytical expressions of the type

$$v(E) = \frac{\mu_0 E}{\left[\left(a + \frac{v_p}{E}\right)\left(\frac{E}{E_p}\right)^b\right]^c} \tag{3}$$

if $E \le E_p$, and

$$v(E) = \frac{\frac{v_p}{E_p} E}{\left[1 + \frac{(E - E_p)^2}{E_c^d}\right]^e} \tag{4}$$

if $E \geq E_p$, where v_p is the peak velocity, E_p is the threshold field, E_c is the critical field, and μ_0 is the ohmic mobility. The parameters a, b, c, d and e represent numerical coefficients. The results of the fitting are reported in Fig. 8. The parameters have been calculated on the basis of MC simulation and are given in Table 1. Instead of using a single formula we used two formulas, one below and one above E_p, in order to better interpolate the curves of the mean velocity and the chord mobility. However, this induces a couple of spikes around E_p. We have also calculated the average drift velocity for different values of electron density. The results are reported in Fig. 9. When doping is higher, scatterings with ionized impurities are more frequent. As a consequence, for a given value of the electric field, the electron velocity is higher when the electron density is lower. In the same figure the measurements of Hasse [43] are reported, and we observe a good agreement.

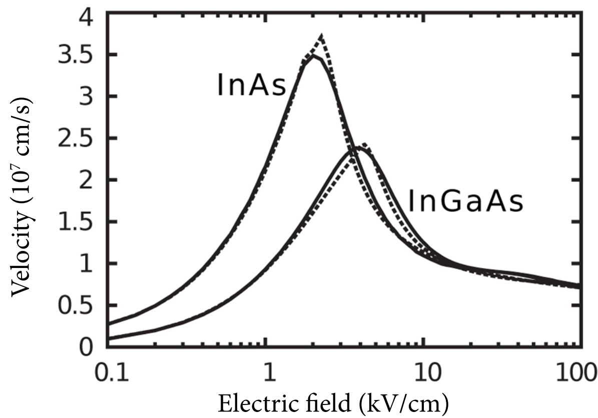

Fig. 8. Average electron velocity as a function of the electric field for InGaAs and InAs, with $N_D = 10^{16}$ cm^{-3}. The continuous line refers to MC simulation and the dotted lines to the analytical formula.

Table 1. Values of the parameters used to fit the drift velocity of $In_{0.53}Ga_{0.47}As$ and InAs with Eqs. (3) and (4).

Parameters	$In_{0.53}Ga_{0.47}As$	InAs
Peak velocity v_p, 10^7 cm/s	2.5	3.3
Threshold field E_p, kV/cm	3.75	2.0
Critical field E_c, kV/cm	1.2	0.6
Ohmic mobility μ_0, m^2/Vs	1.0	2.2
a	1	0.9
b	2.5	2.5
c	1.02	0.15
d	2.01	2.02
e	0.51	0.56

7. Mobility

Figure 10 represents the electron static chord mobility as a function of the electric field for different concentrations of the ionized impurities, for both InAs and InGaAs. We remark that the chord mobility decreases with the electric field while remaining positive. We can see that InAs is able to reach a higher velocity for a given electric field, and is thus characterized by a much higher mobility than that of InGaAs: the maximum ohmic mobility in the case of InGaAs is 10 000 cm^2/Vs, whereas the ohmic mobility

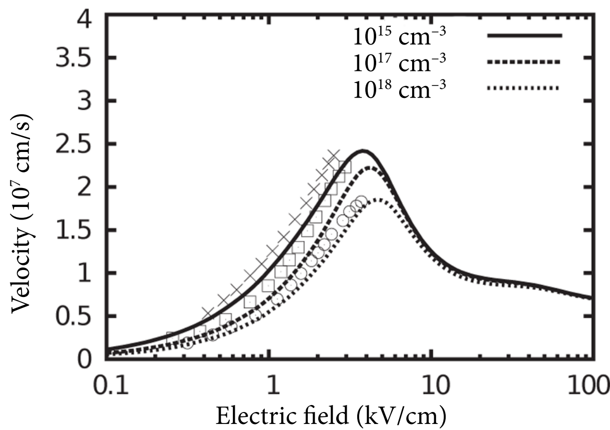

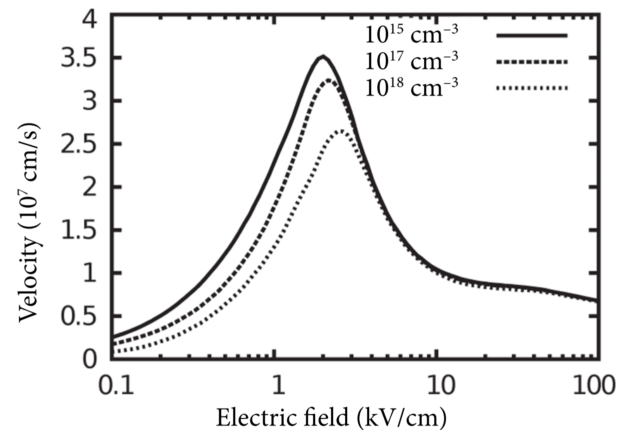

Fig. 9. Average drift velocity as a function of the electric field in InGaAs (left) and InAs (right) for different values of electron density. The lines represent MC simulations, and the symbols show the experimental results of Hasse [43]. The dotted lines simply connect the reported points.

can reach 23 000 cm^2/Vs in the case of InAs. The values of ohmic mobility for the other concentrations are reported in Table 2. However, as previously observed for the velocity, the chord mobility decreases as the density of ionized impurities increases. In Fig. 11 we have also compared our MC results of the ohmic mobility versus the electron density with those already present in the literature [52, 53]. Finally, in Fig. 12 we have reported the electron static differential mobility versus electric field for different electron densities. For low values of the electric field, mobility remains almost constant and equal to the chord mobility. For a greater electric field, a negative differential mobility appears due to inter-valley transfer and to the fact that the electrons in the Γ valley have a higher mobility because of their low effective mass, whereas carriers in higher valleys have a higher effective mass and thus a lower mobility. This negative differential mobility observed for high electric fields is one of the typical characteristics of III–V compounds.

Table 2. Ohmic mobility for InGaAs and InAs for different electron densities.

Electron density, cm^{-3}	μ_0, m^2/Vs, $In_{0.53}Ga_{0.47}As$	μ_0, m^2/Vs, InAs
10^{16}	1.0	2.3
10^{17}	0.75	1.8
10^{18}	0.58	1.3

By dividing the velocity fitting formula by the electric field (see Eqs. (3) and (4)) we obtain analytical expressions for the chord mobility. The results are reported in Fig. 13 and show a good agreement with the MC simulation.

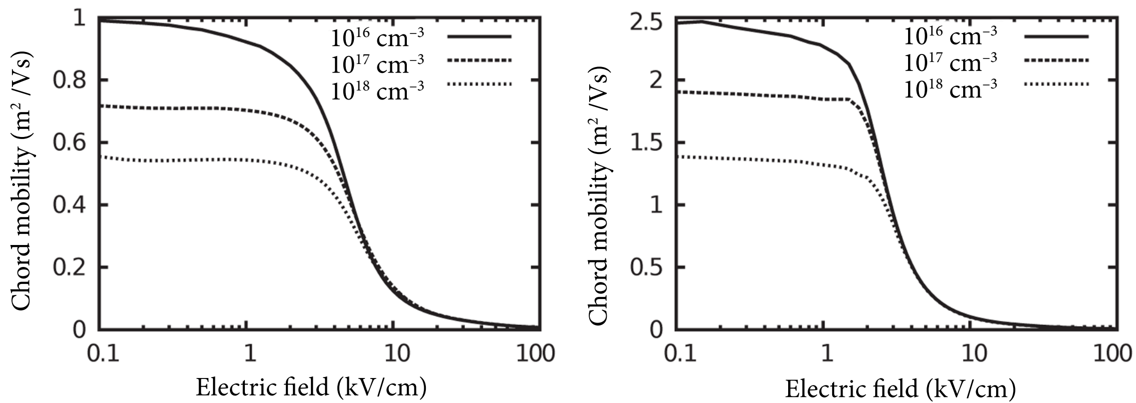

Fig. 10. Chord mobility as a function of the electric field for different concentrations electron density in InGaAs (left) and InAs (right).

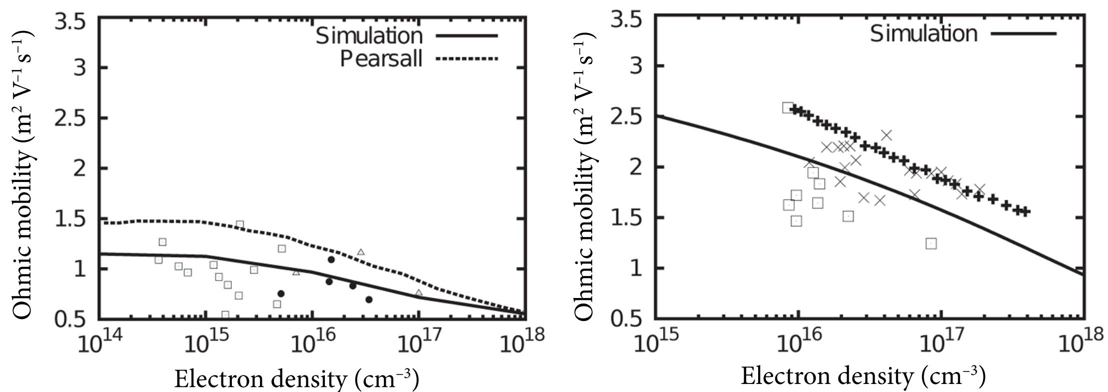

Fig. 11. Ohmic mobility as a function of electron density for InGaAs (left) and InAs (right). The continuous lines represent MC simulation and the points are different experimental results of Pearsall [52] and Karataev [53].

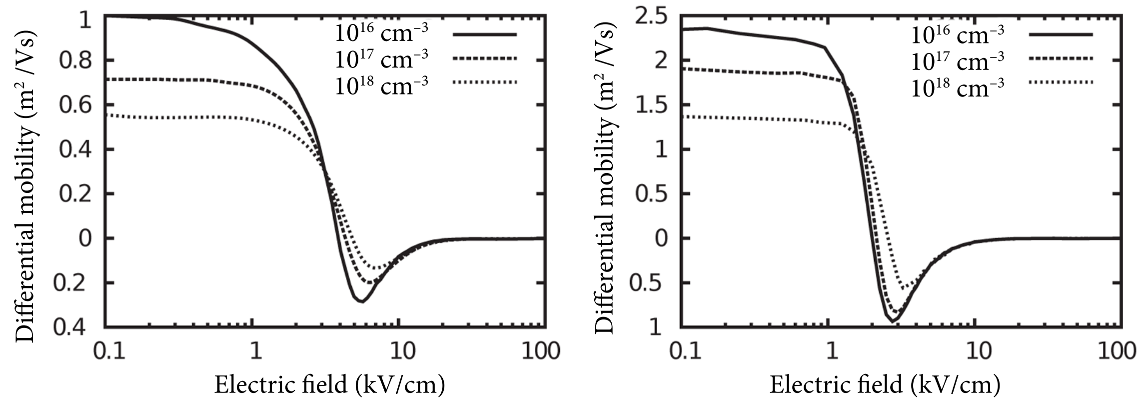

Fig. 12. Differential mobility as a function of the electric field for different electron densities in InGaAs (left) and InAs (right).

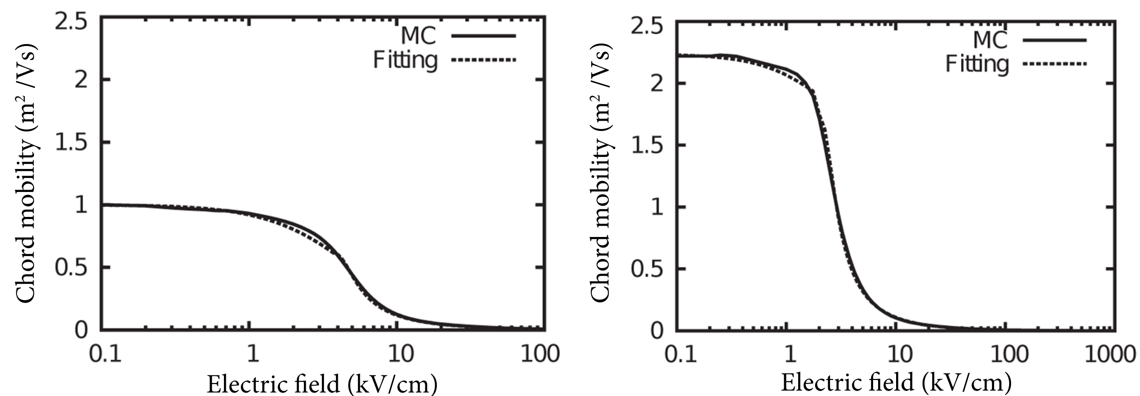

Fig. 13. Chord mobility as a function of the electric field in InGaAs (left) and InAs (right), with $N_D = 10^{16}$cm^{-3}. The continuous lines refer to MC simulation and the dotted line to the analytical formula.

8. Conclusions

After a description of the theoretical model, we have presented a review of stationary electron transport in $In_{0.53}Ga_{0.47}As$ and InAs obtained by a Monte Carlo simulation of the bulk materials under stationary and homogeneous conditions. The main transport parameters, i.e. valley population, effective mass, average energy, drift velocity and mobility (ohmic and differential), have been analyzed as functions of the applied electric field and electron density. When possible, our simulations have been compared to several experimental and theoretical results in order to estimate the dispersion of the data available in the literature. Additionally, we have provided the parameters for an analytical fitting of the drift velocity and mobility to ensure an easy implementation in macroscopic simulations such as drift diffusion and hydrodynamic approaches. The obtained results confirm excellent transport properties of both materials for their implementation in modern electronic devices with a general improving of the performances expected in the case of InAs.

References

[1] R. Waser, *Nanoelectronics and Information Technology* (Wiley-VCH Verlag GmbH & Co. KGaA, Weinheim, 2003).

[2] T. Suemitsu, T. Ishii, H. Yokoyama, Y. Umeda, T. Enoki, Y. Ishii, and T. Tamamura, 30-nm-gate InAlAs/InGaAs HEMTs lattice-matched to InP substrates, IEDM Tech. Dig. 223–226 (1998).

[3] T. Suemitsu, H. Yokoyama, T. Ishii, T. Enoki, G. Meneghesso, and E. Zanoni, 30-nm two-step recess gate InP-based InAlAs/InGaAs HEMTs, IEEE Trans. Electron Dev. **49**, 1694 (2002).

[4] K. Shinohara, Y. Yamashita, A. Endoh, I. Watanabe, K. Hikosaka, T. Matsui, T. Mimura, and S. Hiyamizu, 547-GHz ft $In_{0.7}Ga_{0.3}As$-$In_{0.52}Al_{0.48}As$ HEMTs with reduced source and drain resistance, IEEE Electron Device Lett. **25**, 241 (2004).

[5] K. Shinohara, Y. Yamashita, A. Endoh, I. Watanabe, K. Hikosaka, T. Mimura, S. Hiyamizu, and T. Matsui, in: *Proceedings of 16th International Conference on Indium Phosphide and Related Materials*, IEEE Catalog 04CH37589 (Kagoshima, Japan, 2004) p. 721.

[6] B. Doyle, R. Arghavani, D. Barlage, M. Datta, S. Doczy, J. Kavalieros, A. Murthy, and R. Chau, Transistor elements for 30 nm physical gate lengths and beyond, Intel. Technol. J. **6**, 42 (2002).

[7] R. Dingle, H.R. Stormer, A.C. Gossard, and W. Wiegmann, Electron mobilities in modulation-doped semiconductor heterojunction superlattices, J. Appl. Phys. **33**, 655 (1978).

[8] T. Mimura, K. Joshin, S. Hiyamizu, K. Kikusaka, and M. Abe, High electron mobility transistor logic, Jpn. J. Appl. Phys. **20**, L598–600 (1981).

[9] J.H. Marsh, Effects of compositional clustering on electron transport in $In_{0.53}Ga_{0.47}As$, Rev. Mod. Phys. **20**, 598 (1981).

[10] W. Knap, F. Teppe, N. Dyakonova, Y.M. Meziani, J. Lusakowsky, L. Varani, and J.F. Millithaler, Terahertz generation and detection by plasma waves in nanometer gate high electron mobility transistors, Acta Phys. Pol. A **107**(1), 82 (2005).

[11] W. Knap, J. Lusakowski, T. Parenty, S. Bollaeret, A. Cappy, and M. Shur, Terahertz emission by plasma waves in 60 nm gate high electron mobility transistors, Appl. Phys. Lett. **84**, 2331–2333 (2004).

[12] M.V. Fischetti, Monte Carlo simulation of transport in technologically significant semiconductors of the diamond and zinc-blende structures – Part I: Homogeneous transport, IEEE Trans. Electron Dev. **38**, 634–649 (1991).

[13] T.H. Windhorn, L.W. Cook, and G.E. Stillman, The electron velocity-field charateristic for n-$In_{0.53}Ga_{0.47}As$ at 300 K, IEEE Electron Device Lett. **3**, 18–20 (1982).

[14] J.L. Thobel, L. Baundry, A. Cappy, P. Bourel, and R. Fauquembergue, Electron transport properties of strained $In_xGa_{1-x}As$, Appl. Phys. Lett. **56**, 346–348 (1990).

[15] P. Borowik and J.L. Thobel, Improved Monte Carlo method for the study of electron transport in degenerate semiconductors, J. Appl. Phys. **84**, 3706–3709 (1998).

[16] A. Ghosal, D. Chattopadhyay, and N.N. Purkait, Hot-electron velocity overshoot in $In_{0.53}Ga_{0.47}$, J. Appl. Phys. **44**, 773–774 (1984).

[17] I.M. Sobol, *The Monte Carlo Method* (Mir Publishers, Moscow, 1975).

[18] C. Jacoboni and L. Reggiani, The Monte Carlo method for the simulation of charge transport in semiconductors with applications to covalent materials, Rev. Mod. Phys. **55**, 645 (1983).

[19] J. Mateos, T. Gonzalez, D. Pardo, V. Hoel, and A. Cappy, Improved Monte Carlo algorithm for the simulation of δ-doped AlInAs/GaInAs HEMTs, IEEE Trans. Electron Dev. **47**, 250 (2000).

[20] K.F. Brennan and D.H. Park, Theoretical comparison of electron real-space transfer in classical and quantum two dimensional heterostructure systems, J. Appl. Phys. **65**, 1156 (1989).

[21] O. Madelung, *Semiconductors: Data Handbook* (Springer, Berlin, 2003).

[22] S. Adachi, *Physical Properties of III–V Semiconductors InGaAsP* (Wiley, New York, 1992).

[23] C. Jacoboni and P. Lugli, *The Monte Carlo Method for Semiconductor Device Simulation* (Springer-Verlag Wien, 1989).

[24] G.M. Dunn, G.J. Rees, J.P.R. David, S.A. Plimmer, and D.C. Herbert, Monte Carlo simulation of impact ionization and current multiplication in short GaAs p^+in^+ diodes, Semicond. Sci. Technol. **12**, 111 (1997).

[25] G.M. Dunn, A. Phillips, and P.J. Topham, Current instability in power HEMTs, Semicond. Sci. Technol. **16**, 562 (2001).

[26] B.G. Vasallo, J. Mateos, D. Pardo, and T. González, Influence of trapping-detrapping processes on shot noise in nondegenerate quasiballistic transport, Semicond. Sci. Technol. **17**, 440 (2002).

[27] K. Kalna and A. Asenov, Gate tunnelling and impact ionisation in sub 100 nm PHEMTs, IEICE Trans. Electron. (Special Issue on the 2002 IEEE International Conference on Simulation of Semiconductor Processes and Devices (SISPAD'02)) **86**(3), 330 (2003).

[28] C.L. Anderson and C.R. Crowell, Threshold energies for electron-hole pair production by impact ionization in semiconductors, Phys. Rev. B **5**, 2267 (1972).

[29] W. Quade, E. Scoll, and M. Ruden, Impact ionization within the hydrodynamic approach to semiconductor transport, Solid State Electron. **36**, 1493 (1993).

[30] T.P. Pearsall, Impact ionization rates for electrons and holes in $Ga_{0.47}In_{0.53}As$, Appl. Phys. Lett. **36**, 218 (1980).

[31] F. Osaka, T. Mikawa, and T. Kanada, Impact ionization coefficients of electrons and holes in (100)-oriented $Ga_{1-x}In_xAsyP_{1-y}$, IEEE J. Quantum Electron. **21**, 1326 (1985).

[32] J. Bude and K. Hess, Thresholds of impact ionization in semiconductors, J. Appl. Phys **72**, 3554 (1992).

[33] G.E. Bulman, V.M. Robbins, G.E. Stillmann, G. Hill, and G.J. Rees, Thresholds of impact ionization in semiconductors, IEEE Trans. Electron Dev. **32**, 2454 (1985).

[34] D.S. Ong, K.Y. Choo, Analytical band Monte Carlo simulation of electron impact ionization in $In_{0.53}Ga_{0.47}As$, J. Appl. Phys. **96**, 5649 (2004).

[35] J.S. Ng, C.H. Tan, J.P.R. David, G. Hill, and G.J. Rees, Thresholds of impact ionization in semi-

conductors, IEEE Trans. Electron Dev. **50**, 901 (2003).

[36] G. Stillmann, *Properties of Lattice-Matched and Strained Indium Gallium Arsenide*, ed. P. Bhattacharya (INSPEC, London, U. K., 1993).

[37] M.P. Mikhailova, A.A. Rogachev, and I.N. Yassievich, Impact ionization and Auger recombination in InAs, Sov. Phys. Semicond. **10**(8), 866–871 (1976).

[38] K. Brennan and K. Hesse, High field transport in GaAs, InP and InAs, Solid State Electron. **27**(4), 347–357 (1984).

[39] K.F. Brennan and N.S. Mansour, Monte Carlo calculation of electron impact ionization in bulk InAs and HgCdTe, J. Appl. Phys. **69**(11), 7844–7847 (1991).

[40] A. Krotkus and Z. Dobrovolskis, *Electrical Conductivity of Narrow-Gap Semiconductors* (Mokslas, Vilnius, 1988).

[41] L. Reggiani, *Topics in Applied Physics. Hot-Electron Transport in Semiconductors*, Vol. 58 (Springer-Verlag Berlin Heidelberg GmbH, 1985).

[42] Y. Hori, Y. Ando, Y. Miyamoto, and O. Sugino, Effect of strain on band structure and electron transport in InAs, Solid State Electron. **43**, 1813–1816 (1999).

[43] M.A. Hasse, N. Robbins, N. Tabatabaie, and G.E. Stillmann, Subthreshold electron velocity-field characteristics of GaAs and $In_{0.53}Ga_{0.47}As$, Solid State Electron. **43**, 1813–1816 (1999).

[44] J.H. Marsh, Effects of compositional clustering on electron transport in $In_{0.53}Ga_{0.47}As$, Appl. Phys. Lett. **41**(8), 732–734 (1982).

[45] W.K. Ng, C.H. Tan, J.P.R. David, P.A. Houston, M. Yee, and J.S. Ng, Temperature dependent low-field electron multiplication in $In_{0.53}Ga_{0.47}As$, Appl. Phys. Lett. **83**(14), 2820–2822 (2003).

[46] M.A. Littlejohn, K.W. Kim, and H. Tian, in: *Properties of Lattice-Matched and Strained Indium Gallium Arsenide*, ed. P. Bhattacharya (INSPEC, London, U. K., 1993) pp. 107–116.

[47] V. Balynas, A. Krotkus, A. Stalnionis, A.T. Gorelionok, N.M. Shmidt, and J.A. Tellefsen, Time-resolved, hot-electron conductivity measurement using an electro-optic sampling technique, Appl. Phys. Lett. **51**(4), 357–360 (1990).

[48] C.H. Tan, G.J. Rees, P.A. Houston, J.S. Ng, W.K. Ng, and J.P.R. David, Temperature dependence of electron impact ionisation in $In_{0.53}Ga_{0.47}As$, Appl. Phys. Lett. **84**, 2322 (2004).

[49] M. Isler, Phonon-assisted impact ionization of electron in $In_{0.53}Ga_{0.47}As$, Phys. Rev. B **63**, 115209 (2001).

[50] G. Satyanadh, R.P. Joshi, N. Abedin, and U. Singh, Monte Carlo calculation of electron drift characteristics and avalanche noise in bulk InAs, J. Appl. Phys. **91**, 1331–1338 (2002).

[51] L. Amer, C. Sayah, B. Bouazza, A. Guen-Bouazza, N.E. Chabane-Sari, and C. Gontrand, Analyse du phénomène de transport électronique dans l'InAs et le GaAs par la méthode de Monte Carlo pour la conception d'un transistor HEMT, in: *CISTEMA'2003* (Université de Tlemcen, 2003).

[52] T.P. Pearsall, *GaInAsP Alloy Semiconductors* (John Wiley & Sons, Chichester, 1982).

[53] V.V. Karataev, M.G. Mil'vidsky, N.S. Rytova, and V.I. Fistui, Compensation in n-type InAs, Sov. Phys. Semicond. **11**(9), 1009–1011 (1977).

ELEKTRONŲ PERNAŠOS TŪRINIUOSE InGaAs IR InAs KAMBARIO TEMPERATŪROJE SAVYBIŲ APŽVALGA

S. Karishy [a], P. Ziadé [a], G. Sabatini [b], H. Marinchio [b], C. Palermo [b], L. Varani [b], J. Mateos [c], T. Gonzalez [c]

[a] *Libano universitetas, Fanaras, Libanas*

[b] *Monpeljė universitetas, Prancūzija*

[c] *Salamankos universitetas, Ispanija*